Mathematical Methods in the Applied Sciences

WILEY

RESEARCH ARTICLE OPEN ACCESS

Analytical and Numerical Soliton Solutions of the Shynaray II-A Equation Using the $\left(\frac{G'}{G}, \frac{1}{G}\right)$-Expansion Method and Regularization-Based Neural Networks

Aamir Farooq[1,2,3] | H. W. A. Riaz[4] | Sadique Rehman[5] | M. Mamun Miah[6] | Wen Xiu Ma[1,7,8,9]

[1]Department of Mathematics, Zhejiang Normal University, Jinhua, PR China | [2]Research Center of Astrophysics and Cosmology, Khazar University, Baku, Azerbaijan | [3]Department of Applied Mathematics and Data Science, Asian University for Women, Chattogram, Bangladesh | [4]Department of Physics, Zhejiang Normal University, Jinhua, PR China | [5]Division of Mathematical and Physical Sciences, Kanazawa University, Kanazawa, Japan | [6]Department of Applied Mathematics, University of Rajshahi, Rajshahi, Bangladesh | [7]Department of Mathematics, King Abdulaziz University, Jeddah, Saudi Arabia | [8]Department of Mathematics and Statistics, University of South Florida, Tampa, Florida, USA | [9]Material Science Innovation and Modelling, North-West University, Mafikeng Campus, Mmabatho, South Africa

Correspondence: Wen Xiu Ma (mawx@cas.usf.edu)

Received: 11 April 2025 | **Revised:** 18 August 2025 | **Accepted:** 22 January 2026

Keywords: Bayesian regularization-backpropagation neural network | $\left(\frac{G'}{G}; \frac{1}{G}\right)$-expansion method | Shynaray-IIA equation | soliton solutions

ABSTRACT

Nonlinear differential equations play a fundamental role in modeling complex physical phenomena across solid-state physics, hydrodynamics, plasma physics, nonlinear optics, and biological systems. This study focuses on the Shynaray II-A equation, a relatively less-explored parametric nonlinear partial differential equation that describes nonlinear wave propagation and soliton dynamics in diverse physical systems. To address the gap in analytical and numerical treatments of this equation, we derive new exact soliton solutions using the $\left(\frac{G'}{G}, \frac{1}{G}\right)$-expansion method, yielding exponential, trigonometric, and rational solution forms. Moreover, we introduce a novel hybrid framework by applying regularization-based backpropagation neural networks to approximate these solutions numerically. This dual approach, combining symbolic analysis with machine learning, offers a robust means to validate and extend analytical findings. The originality of this work lies in presenting, for the first time, a unified analytical-neural network framework for solving the Shynaray II-A equation, which has not been systematically studied in prior literature. Comparative error metrics and visualization confirm the accuracy and efficiency of the proposed method, providing new insights into the behavior of nonlinear wave systems and demonstrating the potential of hybrid soliton modeling strategies.

1 | Introduction

In exploring the nonlinear aspects of the analytical frameworks, nonlinear partial differential equations are of utmost significance. The nonlinear coupled Shynaray-IIA equation shows excellent promise in modeling complex wave phenomena.

https://doi.org/10.1002/mma.70566

This includes, but is not limited to, plasma physics, fiber optics, mathematical physics, and telecommunications engineering. For the nonlinear processes, these equations are vital because they enable the analysis of otherwise complex systems to be understood. The Shynaray-IIA equation is an integrable system of coupled differential equations that support soliton solutions. It can be formally written down in the following manner [1, 2]:

$$\begin{aligned} i\frac{\partial \phi}{\partial t} + \frac{\partial^2 \phi}{\partial x \partial t} - i(\psi\phi)_x &= 0, \\ i\Xi - \frac{\partial^2 \Xi}{\partial x \partial t} - i(\psi\Xi)_x &= 0, \\ \frac{\partial \psi}{\partial x} - \frac{\ell^2}{p}\frac{\partial(\Xi\phi)}{\partial t} &= 0. \end{aligned} \tag{1.1}$$

In the above system (1.1), the last equation is changed into the following form by utilizing $\Xi = \zeta\overline{\phi}(\zeta = \pm 1)$,

$$\begin{aligned} i\frac{\partial \phi}{\partial t} + \frac{\partial^2 \phi}{\partial x \partial t} - i(\psi\phi)_x &= 0, \\ \frac{\partial \psi}{\partial x} - \frac{\ell^2\zeta}{p}\frac{\partial(|\phi|^2)}{\partial t} &= 0. \end{aligned} \tag{1.2}$$

In (1.2), the parameters ℓ, ζ, and p play important physical roles. The parameter ℓ governs the strength of the nonlinear coupling between the auxiliary field ψ and the intensity $|\phi|^2$. The sign parameter $\zeta = \pm 1$ distinguishes between focusing ($\zeta = +1$) and defocusing ($\zeta = -1$) nonlinearities. The parameter p acts as a normalizing constant, with physical significance linked to the amplitude scaling and energy distribution of the wave field ϕ. These parameters can be interpreted analogously to coefficients found in models of optical fibers, plasma, or shallow water wave systems, where the balance between dispersion and nonlinearity determines the propagation characteristics of localized structures such as solitons. To examine the linear wave dynamics of the Shynaray-IIA equation, we consider a plane wave solution:

$$\phi(x,t) = \epsilon\ e^{i(kx-\omega t)}, \tag{1.3}$$

while treating $\psi(x,\ t)$ as a real-valued field. From the second equation of (1.2), we have

$$\psi_x = \frac{\ell^2\zeta}{p}\frac{\partial}{\partial t}(|\phi|^2). \tag{1.4}$$

Since $|\phi|^2 = \epsilon^2$ is the constant, it follows that $\psi_x = 0$, and hence $\psi = \Psi_0 \in \mathbb{R}$ is a constant background.

Substituting ϕ and constant ψ into the first equation yields:

$$\omega = \frac{-k\Psi_0}{1+k}, \quad k \neq -1. \tag{1.5}$$

This defines a dispersion relation with a singularity at $k = -1$. The corresponding group velocity is

$$v_g = \frac{-\Psi_0}{(k+1)^2}, \tag{1.6}$$

showing strong dispersion whose sign and magnitude depend on the real background level Ψ_0. These dispersive effects are counterbalanced by the nonlinear terms, leading to the formation of stable soliton structures, as derived in Section 3.1.

Research on optical solitons in nonlinear media is a major focus. Optical solitons, the stable and self-sustained wave packets, play a vital role in high-speed data transfer in optical fibers and all optical switches [3]. They enhance the functionality and reliability of modern telecommunication systems, given their ability to retain shape and strength over long distances. This area of research aims to improve our understanding of soliton dynamics and their applications in technology, enabling advances in communication systems.

This subject, along with many other areas in mathematics and physics, is still being researched actively. The analysis of closed-form soliton solutions for nonlinear partial differential equations remains essential for thoroughly examining nonlinear processes and practical problem-solving. New developments in nonlinear science have yielded numerous innovative methods for deriving closed-form solutions to these equations. For example, an arbitrary parametric method was applied to find analytic solutions for generalized nonlinear Schrödinger equations with cubic-quintic nonlinearity and self-steepening [4]. The homoclinic test and the modified homoclinic trial methods were used to yield exact kink-wave solutions, doubly periodic solutions, and periodic solitons for the Kadomtsev-Petviashvili equation [5].

Several well-established techniques are widely applied to derive such solutions, including the $\left(\frac{G'}{G}\right)$-expansion method [6, 7], the Riccati equation method [8], the improved generalized Riccati equation mapping method [9], the ϕ^6-model expansion method [10], the improved tan $(\phi/2)$-expansion method [11], the improved generalized Riccati equation mapping method [9], the modified simple equation techniques [12–14], the unified algebraic method [15], the intermediary Jacobi's elliptic function [16], the Sardar sub-equation method [17, 18], the trial equation method [13, 19, 20], the extended direct algebraic method [21], the Kudryashov's simplest method [22] and many more methods. Those approaches are being constantly improved and generalized, providing tools for doing research on nonlinear systems. $\left(\frac{G'}{G}\right)$-expansion method is one of them that was recently developed in the field of nonlinear partial differential equations. This pioneering method is an elegant and efficient approach that establishes a general framework for solving thousands of nonlinear partial differential equations, and thus is one of the most general ones in all these fields of advanced studies. This approach has potential, and a few recent studies report good results, but it has not been widely applied. For instance, Li et al. [18, 23] introduced the two-variable $\left(\frac{G'}{G}, \frac{1}{G}\right)$−expansion method, enabling the discovery of various traveling wave solutions for the Zakharov equations, which have proven invaluable in furthering analytical investigations. Additionally, this method has facilitated significant progress in solving other nonlinear equations. For example, rational, complex trigonometric, hyperbolic, and trigonometric traveling wave solutions were derived for the Jimbo-Miwa equation in higher-dimensional settings using this approach. Some scholars have explored the solutions of the Shynaray-IIA equation [9]. Faridi et al. [24] have recently established the periodic, bell-shaped, anti-bell-shaped, M-shaped, and W-shaped soliton solutions of the Shynaray-IIA equation. The obtained solutions can explain several complex nonlinear phenomena, including tidal waves and tsunamis. Currently, in [25, 26], researchers have invented many other closed-form solutions of the Shynaray-IIA equation.

Recent advancements in computational capabilities have revolutionized the development of simulations and approaches to solving both traditional and contemporary challenges, with artificial neural networks (ANNs) emerging as a significant tool in mathematical modeling. ANNs have been developed in response to the functioning of the human brain, which includes interconnected neurons with several layers that produce outputs from inputs, such as predictions or classifications. Diffusion models have applications in natural language processing, pattern recognition, time series analysis, supervised learning, unsupervised learning, and reinforcement learning. However, despite their many uses, ANNs have some issues that can prevent this, such as high computational cost, dependency on large data sets, sensitivity to noisy and incomplete data, and the ability to overfit, reducing their generalization ability. As such, those limitations highlight the necessity of developing ANN frameworks that can produce sound mathematical models and solve problems as such. ANNs were first proposed by McCulloch and Pitts in 1943 [27]. Since then, theoretical research has played a massive role in realizing ANNs as a universal function approximation framework [28, 29]. Li et al., for example, conducted studies in which they showed that ANNs would approximate multivariable functions and all their derivatives with high accuracy (at real scales) to low complexity, often fewer than three hidden layers and twenty neurons per layer in Nguyen-Thien [30] and TranCong [31]. Physics-informed neural networks (PINNs), introduced by Raissi et al. [32], have significantly expanded the application of ANNs to solve partial differential equations and tackle complex mathematical and physical problems. Many studies have applied artificial neural networks to various mathematical models. Riaz et al. [33, 34] investigated solitonic solutions for the reduced Maxwell-Bloch equations and the time-dependent $(2+1)$-dimensional modified KdV equation using the Darboux transformation and ANNs. They initially derived the soliton solutions using the Darboux transformation and then trained these solutions with an ANN. Waheed et al. [35] explored peakon and solitary wave solutions for the Lax equation using the Levenberg-Marquardt-ANN method. Jayesh et al. [36] studied liquid droplet entrainment in an annular flow boiling regime with the Bayesian regularization-backpropagation neural network (BR-BPNN). Kumar et al. [37] applied ANNs to investigate the multi-physics of double-diffusion convective motion in an inverted cylinder-like permeable container. For additional applications of ANNs, see the references [33–37].

Motivated by the gaps identified in the existing literature, this study is the first to integrate the $\left(\frac{G'}{G}, \frac{1}{G}\right)$-expansion method with a BR-BPNN to analyze the Shynaray II-A equation. This integration establishes a robust and flexible computational framework: the $\left(\frac{G'}{G}, \frac{1}{G}\right)$-expansion technique provides exact soliton solutions with explicit analytical structure, while BR-BPNN enables accurate approximation of these solutions under noisy or limited-data conditions. Since BR-BPNN is a supervised learning model requiring both inputs and outputs, the analytically derived solutions from the expansion method serve as high-quality synthetic training data. While the $\left(\frac{G'}{G}, \frac{1}{G}\right)$-expansion method is limited to equations that admit such transformations, coupling it with BR-BPNN extends its utility by enabling numerical solution generation and robustness analysis.

The primary motivations for solving Equation (1.2) using this hybrid approach are as follows:

- To investigate Equation (1.2) via intelligent stochastic computing techniques, particularly BR-BPNN, for obtaining data-driven approximate solutions.
- To leverage the $\left(\frac{G'}{G}, \frac{1}{G}\right)$-expansion method to generate synthetic training datasets for BR-BPNN.
- To evaluate the predictive performance and robustness of BR-BPNN using comprehensive statistical error analysis for Equation (1.2).

The subsequent sections of the manuscript are structured as follows: Section 2 outlines the comprehensive methodology of the $\left(\frac{G'}{G}, \frac{1}{G}\right)$–expansion approach and the BR-BPNN. In Section 3, explicit expressions for the exact solutions of (1.2) are derived using the $\left(\frac{G'}{G}, \frac{1}{G}\right)$– expansion method. This is followed by applying the BR-BPNN to achieve results for (1.2). Section 4 presents a graphical representation of the solutions for (1.2), derived using the $\left(\frac{G'}{G}, \frac{1}{G}\right)$– expansion method in conjunction with the BR-BPNN. In conclusion, Section 5 summarizes the paper's findings.

2 | Methods

The following outlines the complete procedure for solving (1.2) using the $\left(\frac{G'}{G}, \frac{1}{G}\right)$-expansion method. Additionally, a brief overview of the application of the BR-BPNN algorithm in analyzing the solutions obtained from the $\left(\frac{G'}{G}, \frac{1}{G}\right)$-expansion method will be provided.

2.1 | $\left(\frac{G'}{G}, \frac{1}{G}\right)$-Expansion Method

This subsection examines the primary formulation steps of the two-variable expansion method $\left(\frac{G'}{G}, \frac{1}{G}\right)$ to derive new optical soliton solutions of (1.2). The auxiliary linear ordinary differential equation is defined as follows:

$$\frac{d^2G}{d\chi^2} + \tau G = \nu. \tag{2.1}$$

where τ and ν are constants. The expression below delineates two parameters:

$$\varkappa = \frac{G'(\chi)}{G(\chi)}, \Omega = \frac{1}{G(\chi)}. \tag{2.2}$$

Therefore, we obtained

$$\varkappa' = -\varkappa^2 + \nu\Omega - \tau, \Omega' = -\varkappa\Omega. \tag{2.3}$$

The solution of (2.1) is relying upon τ and is categorized into three distinct cases:

Case 1. When $\tau < 0$, the general solution of (2.1),

$$G = S_1 \sinh(\sqrt{-\tau}\chi) + S_2 \cosh(\sqrt{-\tau}\chi) + \frac{\nu}{\tau}, \tag{2.4}$$

where S_1 and S_2 represent two optional constants. Subsequently, we have

$$\Omega^2 = \frac{-\tau(\varkappa^2 - 2\nu\Omega + \tau)}{\tau^2\omega_1 + \nu^2} \quad \text{and} \quad \omega_1 = S_1^2 - S_2^2. \tag{2.5}$$

Case 2. When $\tau > 0$, the general form for the solution of (2.1),

$$G = S_1 \sin(\sqrt{\tau}\chi) + S_2 \cos(\sqrt{\tau}\chi) + \frac{\nu}{\tau}, \tag{2.6}$$

hence, we have

$$\Omega^2 = \frac{\tau(\varkappa^2 - 2\nu\Omega + \tau)}{\tau^2\omega_2 - \nu^2} \quad \text{and} \quad \omega_2 = S_1^2 + S_2^2. \tag{2.7}$$

Case 3. When $\tau = 0$, the general form for the solution of (2.1),

$$G = \frac{\nu}{2}\chi^2 + S_1\chi + S_2, \tag{2.8}$$

Thus, we have

$$\Omega^2 = \frac{(\varkappa^2 - 2\nu\Omega)}{S_1^2 - 2\nu^2 S_2}. \tag{2.9}$$

Take the non-linear evolution equation in four independent constraints x, y, z and t in the below polynomial

$$K(u, u_t, u_x, u_y, u_z, u_{tt}, u_{xx}, u_{yy}, u_{zz}, u_{xy}, u_{xt}, \ldots) = 0, \tag{2.10}$$

Here, we utilized the subscripts to describe the partial derivatives (for instance: $u_t = \frac{\partial u}{\partial t}, u_{tt} = \frac{\partial^2 u}{\partial t^2}$, etc.) and substituted a new wave parameter χ that coincided with the independent constraints as follows:

$$u(x, y, z, t) = u(\chi), \chi = x + y + z - at. \tag{2.11}$$

Considering (2.11) into (2.10), an ODE for $u(\chi)$ transfer as,

$$Q(u, -au', u', u', u', a^2u'', u'', u'', u'', u'', -au'', \ldots) = 0, \tag{2.12}$$

where a denotes the velocity of wave and Q stands for the polynomial of $u(\chi)$ and its corresponding derivatives. Suppose that, with the help of two constraints and the $\left(\frac{G'}{G}, \frac{1}{G}\right)$–expansion method, the solution of the ODE (2.12) has the following form:

$$u(\chi) = \sum_{i=0}^{J} d_i \Phi^i(\chi) + \sum_{i=1}^{J} e_i \Phi^{i-1}(\chi)\xi(\chi). \tag{2.13}$$

Here d_i, e_i are constants, and the positive integer J is said to be the homogeneous balance number. Now, we acquired the optional constants by implementing the two constraints, the $\left(\frac{G'}{G}, \frac{1}{G}\right)$–expansion method. Further details of the process are present in references [23, 38–40].

2.2 | Bayesian Regularization-Backpropagation Neural Network (BR-BPNN)

This subsection outlines the BR-BPNN framework used for learning and approximating analytical soliton solutions. The BR-BPNN algorithm combines classical backpropagation with Bayesian regularization to improve generalization performance and mitigate overfitting, especially in cases with noisy data or limited training samples [41–43].

Let the training dataset T contain m_i pairs of input and target vectors:

$$T = \{(\mathbf{x}_1, \mathbf{t}_{o1}), (\mathbf{x}_2, \mathbf{t}_{o2}), \ldots, (\mathbf{x}_{m_i}, \mathbf{t}_{om_i})\},$$

where each $\mathbf{x}_i$ is a multi-dimensional input vector (e.g., spatial and temporal coordinates), and $\mathbf{t}_{oi}$ represents the corresponding output from the analytical soliton solution. The neural network consists of an input layer, multiple hidden layers with nonlinear activation functions (typically tanh), and an output layer. Let $\boldsymbol{\theta}$ represent the vector of all trainable weights and biases, and $\hat{\mathbf{t}} = \text{net}(\mathbf{x}; \boldsymbol{\theta})$ be the network's predicted output. The residual vector is then $\mathbf{r} = \hat{\mathbf{t}} - \mathbf{t}_o$. The objective is to minimize the error between the predicted and true values using a loss function. In BR-BPNN, the loss function incorporates a regularization term:

$$\mathscr{F}(\boldsymbol{\theta}) = \beta E_T + \alpha E_w, \tag{2.14}$$

where $E_T = \|\mathbf{r}\|_2^2$ is the sum of squared errors, $E_w = \|\boldsymbol{\theta}\|_2^2$ is the sum of squared network weights, and α, β are regularization parameters controlling the trade-off between fitting accuracy and model complexity. Under the Bayesian framework, the posterior probability of the weights is expressed as

$$P(\boldsymbol{\theta}|T, \alpha, \beta) = \frac{\exp(-\mathscr{F}(\boldsymbol{\theta}))}{Z}, \tag{2.15}$$

with Z being the normalization constant derived from Gaussian assumptions on both the noise and weight priors. The training algorithm relies on the Gauss-Newton approximation for second-order optimization. At each iteration, the weights are updated as:

$$\boldsymbol{\theta}_{k+1} = \boldsymbol{\theta}_k - \left(\mathbf{J}^T\mathbf{J} + \mu\mathbf{I}\right)^{-1}\mathbf{J}^T\mathbf{r}, \tag{2.16}$$

where $\mathbf{J}$ is the Jacobian matrix of partial derivatives $\partial\hat{\mathbf{t}}/\partial\boldsymbol{\theta}$, and μ is the damping factor defined as $\mu = \alpha/\beta$. To estimate the optimal regularization parameters, the number of effective parameters γ is introduced:

$$\gamma = P - \alpha \cdot tr\left((\mathbf{J}^T\mathbf{J} + \mu\mathbf{I})^{-1}\mathbf{J}^T\mathbf{J}\right),$$

where P is the total number of trainable weights and biases. The hyperparameters are then updated as follows [44]:

$$\alpha = \frac{\gamma}{2E_w}, \quad \beta = \frac{M-\gamma}{2E_T}, \quad \mu = \frac{\alpha}{\beta}.$$

Training continues until a stopping criterion is met, such as convergence of the loss, gradient threshold, or early stopping based on validation loss. Once trained, the BR-BPNN provides smooth and generalizable approximations of the analytical soliton profiles, validated through visual inspection and error metrics.

3 | Application of $\left(\frac{G'}{G}, \frac{1}{G}\right)$– Expansion Method and the Bayesian Regularization-Backpropagation Neural Network

In this section, we apply the $\left(\frac{G'}{G}, \frac{1}{G}\right)$– expansion method and the BR-BNN to solve the system (1.2). The system (1.2) is solved using these hybrid methods, and their corresponding solutions are analyzed in detail.

3.1 | Application of $\left(\frac{G'}{G}, \frac{1}{G}\right)$– Expansion Method

To acquire the generalized soliton solutions of (1.2) by using $\left(\frac{G'}{G}, \frac{1}{G}\right)$– expansion method, we need to utilize the following transformations:

$$\phi(x,t) = T(\chi)e^{i\varepsilon(x,t)}, \quad \psi(x,t) = H(\chi), \quad \varepsilon(x,t) = -\varpi x + ϝt + \Upsilon, \chi = x - at. \tag{3.1}$$

The ϖ, Υ, and $ϝ$ estimations show the velocity, phase constant, and wave number. After the insertion of (3.1) into (1.2), a result was acquired:

$$aT'' + ϝ(1-\varpi)T + \varpi HT + i(ϝ - a(1-\varpi))T' - HT' - H'T = 0, \tag{3.2}$$

$$H' + \frac{2a\zeta\ell^2}{p}TT' = 0. \tag{3.3}$$

The second equation of the above system was integrated once, and we acquired

$$H(\chi) = -\frac{a\zeta\ell^2}{p}T^2(\chi). \tag{3.4}$$

Inserting (3.4) into the first (1.2) of the system and acquiring the real part as

$$aT'' + ϝ(1-\varpi)T - \frac{\varpi\zeta a\ell^2}{p}T^3 = 0, \tag{3.5}$$

so the balancing number, $J=1$, the solution of (3.5) is considered in the following form:

$$T(\chi)=d_0+d_1\varkappa(\chi)+e_1\Omega(\chi), \tag{3.6}$$

where d_0, d_1 and e_1 are constants to consider, and we explore three types:

Type 1. For hyperbolic function ($\tau<0$)

Substituting (3.6) with (2.3) and (2.5) into (3.5), considering the whole coefficients of the polynomial in $\varkappa$ and Ω, and setting it to zero, we obtain a system of algebraic equations. After solving the system through symbolic computation, we acquire the following estimations of constants:

$$d_0=0, d_1=\pm\frac{\sqrt{p}}{\ell\sqrt{2\varpi\zeta}}, e_1=\pm\frac{\sqrt{p(\omega_1\tau^2+\nu^2)}}{\ell\sqrt{-\tau}\sqrt{2\varpi\zeta}}, a=\frac{2(-\digamma+\varpi\digamma)}{\tau}.$$

Substituting these parameter estimates into (3.6) yields

$$T(\chi)=\pm\frac{\sqrt{p}}{\ell\sqrt{2\varpi\zeta}}\varkappa(\chi)\pm\frac{\sqrt{p(\omega_1\tau^2+\nu^2)}}{\ell\sqrt{-\tau}\sqrt{2\varpi\zeta}}\Omega(\chi), \tag{3.7}$$

Using (2.2) and (2.4), then we achieve

$$\begin{aligned}T(\chi)=&\pm\frac{\sqrt{-p\tau}(S_1\cosh(\sqrt{-\tau}\chi)+S_2\sinh(\sqrt{-\tau}\chi))}{\ell\sqrt{2\varpi\zeta}\left(S_1\sinh(\sqrt{-\tau}\chi)+S_2\cosh(\sqrt{-\tau}\chi)+\frac{\nu}{\tau}\right)}\\&\pm\frac{\sqrt{p(\omega_1\tau^2+\nu^2)}}{\ell\sqrt{-\tau}\sqrt{2\varpi\zeta}\left(S_1\sinh(\sqrt{-\tau}\chi)+S_2\cosh(\sqrt{-\tau}\chi)+\frac{\nu}{\tau}\right)}.\end{aligned} \tag{3.8}$$

Then the solution of (1.2) as follows,

$$\begin{aligned}\phi(x,t)=&\left(\pm\frac{\sqrt{-p\tau}(S_1\cosh(\sqrt{-\tau}(x-at))+S_2\sinh(\sqrt{-\tau}(x-at)))}{\ell\sqrt{2\varpi\zeta}\left(S_1\sinh(\sqrt{-\tau}(x-at))+S_2\cosh(\sqrt{-\tau}(x-at))+\frac{\nu}{\tau}\right)}\right.\\&\left.\pm\frac{\sqrt{p(\omega_1\tau^2-\nu^2)}}{\ell\sqrt{-\tau}\sqrt{2\varpi\zeta}\left(S_1\sinh(\sqrt{-\tau}(x-at))+S_2\cosh(\sqrt{-\tau}(x-at))+\frac{\nu}{\tau}\right)}\right)e^{i(\Upsilon-\varpi x+\digamma t)},\end{aligned} \tag{3.9}$$

$$\begin{aligned}\psi(x,t)=-\frac{a\zeta\ell^2}{p}&\left(\pm\frac{\sqrt{-p\tau}(S_1\cosh(\sqrt{-\tau}(x-at))+S_2\sinh(\sqrt{-\tau}(x-at)))}{\ell\sqrt{2\varpi\zeta}\left(S_1\sinh(\sqrt{-\tau}(x-at))+S_2\cosh(\sqrt{-\tau}(x-at))+\frac{\nu}{\tau}\right)}\right.\\&\left.\pm\frac{\sqrt{p(\omega_1\tau^2-\nu^2)}}{\ell\sqrt{-\tau}\sqrt{2\varpi\zeta}\left(S_1\sinh(\sqrt{-\tau}(x-at))+S_2\cosh(\sqrt{-\tau}(x-at))+\frac{\nu}{\tau}\right)}\right)^2.\end{aligned} \tag{3.10}$$

As a special form, we set $S_2=0, S_1\neq 0$ and $\nu=0$, then the result as follows:

$$\phi(x,t)=\left(\pm\frac{\sqrt{-p\tau}(\coth(\sqrt{-\tau}(x-at)))}{\ell\sqrt{2\varpi\zeta}}\pm\frac{\sqrt{-p\tau}\ csch(\sqrt{-\tau}(x-at))}{\ell\sqrt{2\varpi\zeta}}\right)e^{i(\Upsilon-\varpi x+\digamma t)},$$

$$\psi(x,t)=-\frac{a\zeta\ell^2}{p}\left(\pm\frac{\sqrt{-p\tau}(\coth(\sqrt{-\tau}(x-at)))}{\ell\sqrt{2\varpi\zeta}}\pm\frac{\sqrt{-p\tau}\ csch(\sqrt{-\tau}(x-at))}{\ell\sqrt{2\varpi\zeta}}\right)^2.$$

Type 2. For trigonometric function ($\tau > 0$)

Implementing (3.6) along with (2.3) and (2.7) into (3.5) and setting the whole coefficients of $\varkappa$ and Ω equal to zero and solving the system of equations, we have the following unknown constants:

$$d_0 = 0, d_1 = \pm\frac{\sqrt{p}}{\ell\sqrt{2\varpi\zeta}}, e_1 = \pm\frac{\sqrt{p(\omega_2\tau^2 - \nu^2)}}{\ell\sqrt{2\varpi\zeta\tau}}, a = \frac{2(-\digamma + \varpi\digamma)}{\tau},$$

Inserting the above values in (3.6) and using (2.2) and (2.6), we have

$$\begin{aligned} T(\chi) = &\pm\frac{\sqrt{p\tau}(S_1\cos(\sqrt{\tau}\chi) - S_2\sin(\sqrt{\tau}\chi))}{\ell\sqrt{2\varpi\zeta}\left(S_1\sin(\sqrt{\tau}\chi) + S_2\cos(\sqrt{\tau}\chi) + \frac{\nu}{\tau}\right)} \\ &\pm\frac{\sqrt{p(\omega_2\tau^2 - \nu^2)}}{\ell\sqrt{2\varpi\zeta\tau}\left(S_1\sin(\sqrt{\tau}\chi) + S_2\cos(\sqrt{\tau}\chi) + \frac{\nu}{\tau}\right)}. \end{aligned}$$

The soliton solution of the system (1.2) as given by,

$$\begin{aligned} \phi(x,t) = &\left(\pm\frac{\sqrt{p\tau}(S_1\cos(\sqrt{\tau}(x-at)) - S_2\sin(\sqrt{\tau}(x-at)))}{\ell\sqrt{2\varpi\zeta}\left(S_1\sin(\sqrt{\tau}(x-at)) + S_2\cos(\sqrt{\tau}(x-at)) + \frac{\nu}{\tau}\right)}\right. \\ &\left.\pm\frac{\sqrt{p(\omega_2\tau^2 - \nu^2)}}{\ell\sqrt{2\varpi\zeta\tau}\left(S_1\sin(\sqrt{\tau}(x-at)) + S_2\cos(\sqrt{\tau}(x-at)) + \frac{\nu}{\tau}\right)}\right)e^{i(\Upsilon - \varpi x + \digamma t)}, \end{aligned} \tag{3.11}$$

$$\begin{aligned} \psi(x,t) = -\frac{a\zeta\ell^2}{p}&\left(\pm\frac{\sqrt{p\tau}(S_1\cos(\sqrt{\tau}(x-at)) - S_2\sin(\sqrt{\tau}(x-at)))}{\ell\sqrt{2\varpi\zeta}\left(S_1\sin(\sqrt{\tau}(x-at)) + S_2\cos(\sqrt{\tau}(x-at)) + \frac{\nu}{\tau}\right)}\right. \\ &\left.\pm\frac{\sqrt{p(\omega_2\tau^2 - \nu^2)}}{\ell\sqrt{2\varpi\zeta\tau}\left(S_1\sin(\sqrt{\tau}(x-at)) + S_2\cos(\sqrt{\tau}(x-at)) + \frac{\nu}{\tau}\right)}\right)^2. \end{aligned} \tag{3.12}$$

In a special form, we set $S_2 = 0, S_1 \neq 0$ and $\nu = 0$, then as the result of (3.12) as follows,

$$\phi(x,t) = \left(\pm\frac{\sqrt{p\tau}(\cot(\sqrt{\tau}(x-at))}{\ell\sqrt{2\varpi\zeta}} \pm \frac{\sqrt{p\tau}(\csc(\sqrt{\tau}(x-at)))}{\ell\sqrt{2\varpi\zeta}}\right)e^{i(\Upsilon - \varpi x + \digamma t)},$$

$$\psi(x,t) = -\frac{a\zeta\ell^2}{p}\left(\pm\frac{\sqrt{p\tau}(\cot(\sqrt{\tau}(x-at))}{\ell\sqrt{2\varpi\zeta}} \pm \frac{\sqrt{p\tau}(\csc(\sqrt{\tau}(x-at)))}{\ell\sqrt{2\varpi\zeta}}\right)^2.$$

Type 3. Rational function ($\tau = 0$)

Similarly, implement (3.6) with (2.3) and (2.8) into (3.5), for all the coefficients of $\varkappa$ and Ω is equal to zero, then we have the constant like below

$$d_0 = 0, d_1 = \pm\frac{\sqrt{p}}{\ell\sqrt{2\zeta}}, e_1 = \pm\frac{\sqrt{p(S_1^2 - 2\nu S_2)}}{\ell\sqrt{2\zeta}}, \varpi = 1,$$

The soliton solution of the system (1.2), utilizing the above constants and (2.3) and (2.8), then we have

$$\Theta(x,t) = \left(\pm \frac{\sqrt{p}(\nu(x-at)+S_1)}{\ell\sqrt{2\zeta}\left(\frac{\nu}{2}(x-at)^2+S_1(x-at)+S_2\right)} \pm \frac{\sqrt{p(S_1^2-2\nu S_2)}}{\ell\sqrt{2\zeta}\left(\frac{\nu}{2}(x-at)^2+S_1(x-at)+S_2\right)} \right) e^{i(\Upsilon-\varpi x+\digamma t)}, \tag{3.13}$$

$$\psi(x,t) = -\frac{a\zeta\ell^2}{p}\left(\pm \frac{\sqrt{p}(\nu(x-at)+S_1)}{\ell\sqrt{2\zeta}\left(\frac{\nu}{2}(x-at)^2+S_1(x-at)+S_2\right)} \pm \frac{\sqrt{p(S_1^2-2\nu S_2)}}{\ell\sqrt{2\zeta}\left(\frac{\nu}{2}(x-at)^2+S_1(x-at)+S_2\right)} \right)^2. \tag{3.14}$$

3.2 | Application of Bayesian Regularization-Backpropagation Neural Network

In this study, we use a neural network with a three-layer architecture where each layer contains ten nodes and apply the BR-BPNN method for training. The network utilizes hyperbolic tangent activation functions throughout all hidden layers to effectively manage non-linear relationships present in the data. The training process consists of different epochs for the different solutions of (1.2), with the dataset divided into 70% allocated for training and 30% for testing purposes. To reduce the risk of overtraining and enhance forecast accuracy, the BR-BPNN algorithm is executed independently for ten iterations. The training process is terminated when one of the following conditions is met: the maximum number of iterations is reached, performance achieves a predetermined quality standard, the error decreases below the specified target, or the Levenberg damping factor surpasses 10^{10}. The computational complexity of the proposed method consists of two key components: the $\left(\frac{G'}{G},\frac{1}{G}\right)$-expansion method and the BR-BPNN. The $\left(\frac{G'}{G},\frac{1}{G}\right)$-expansion method is analytical and algebraic in nature, resulting in minimal computational cost, whereas the BR-BPNN framework involves iterative Bayesian updates of α, β, and μ, and has a computational complexity of $\mathcal{O}(n^3+n^2m)$ due to the Gauss–Newton Hessian approximation and matrix inversion steps during training. Despite this higher cost, BR-BPNN offers better generalization and reduces the risk of overfitting, making it well-suited for high-accuracy applications. The performance of the network is assessed through statistical metrics outlined in Table 1, which evaluate the model's effectiveness at various times. The network architecture, training pipeline, and hyperparameter updates, including Bayesian regularization of α, β, and μ, are fully illustrated in the BR-BPNN flowchart Figure 1 for clarity and reproducibility.

TABLE 1 | Statistical metrics employed to evaluate the predictive performance of the solution to (1.2).

Statistical metrics	Range	Optimal value
$\mathrm{RMSE}=\sqrt{\frac{1}{n}\sum_{i=1}^{n}\left(\mathbf{h}_i-\hat{\mathbf{h}}_i\right)^2}$	$0\leq \mathrm{RMSE}<\infty$	0
$\mathrm{MAE}=\frac{1}{n}\sum_{i=1}^{n}\left\lvert\mathbf{h}_i-\hat{\mathbf{h}}_i\right\rvert$	$0\leq \mathrm{MSE}<\infty$	0
$\mathrm{MAPE}=\frac{1}{n}\sum_{i=1}^{n}\left\lvert\frac{\mathbf{h}_i-\hat{\mathbf{h}}_i}{\mathbf{h}_i}\right\rvert$	$0\leq \mathrm{MAPE}<\infty\%$	0%
$\mathrm{MSE}=\frac{1}{n}\sum_{i=1}^{n}\left(\mathbf{h}_i-\hat{\mathbf{h}}_i\right)^2$	$0\leq \mathrm{MSE}<\infty$	0
$\mathrm{R}^2=1-\frac{\sum_{i=1}^{n}\left(\mathbf{h}_i-\hat{\mathbf{h}}_i\right)^2}{\sum_{i=1}^{n}\left(\mathbf{h}_i-\mu_1\right)^2}$	$-1\leq R^2\leq 1$	1
$\mathrm{R}=\frac{\sum_{i=1}^{n}\left(\mathbf{h}_i-\bar{\mathbf{h}}\right)\left(\mathbf{h}_i-\hat{\mathbf{h}}_i\right)}{\sqrt{\sum_{i=1}^{n}\left(\mathbf{h}_i-\bar{\mathbf{h}}\right)^2}\sqrt{\sum_{i=1}^{n}\left(\mathbf{h}_i-\hat{\mathbf{h}}_i\right)^2}}$	$-1\leq R\leq 1$	1
$\mathrm{rSD}=\frac{sd(\mathbf{h})}{sd(\hat{\mathbf{h}})}$	$-\infty\leq \mathrm{rSD}<\infty$	1
$\mathrm{NSE}=1-\frac{\sum_{i=1}^{n}\left(\mathbf{h}_i-\hat{\mathbf{h}}_i\right)^2}{\sum_{i=1}^{n}(\mathbf{h}_i-\bar{\hat{\mathbf{h}}})^2}$	$-\infty\leq \mathrm{NSE}<1$	1

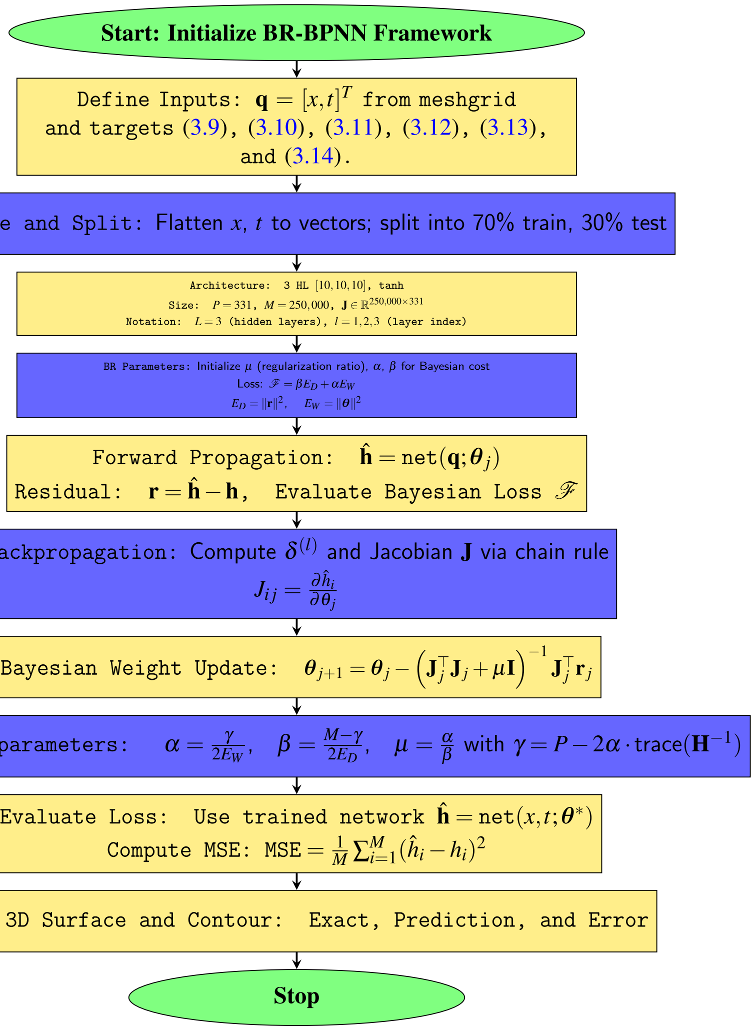

FIGURE 1 | Flowchart illustrating the BR-BPNN training framework for approximating soliton solutions. [Colour figure can be viewed at wileyonlinelibrary.com]

Where RMSE is the root mean square error, MAE is the mean absolute error, MAPE is the mean absolute percentage error, MSE is the mean square error, R^2 is the coefficient of determination, R is the correlation coefficient, rSD is the ratio of standard deviation, NSE is the Nash–Sutcliffe efficiency, n is the number of observations, $\mathbf{h}_i$ denotes the exact solution evaluated at various data points, $\hat{\mathbf{h}}_i$ denotes the predicted solution evaluated at various data points, and μ_1 is the mean of the data.

4 | Graphical Discussion

This section evaluates the performance of the proposed BR-BPNN framework in approximating the analytical soliton solutions of the system (1.2). The exact solutions used for training and testing, given by Equations (3.9), (3.10), (3.11), (3.12), (3.13), and (3.14), were derived using the $\left(\frac{G'}{G}, \frac{1}{G}\right)$-expansion method. All data used in this study were synthetically generated from these analytical expressions using different spatial and temporal discretizations tailored to each experimental scenario. No external or empirical datasets were used. All simulations, including data generation, BR-BPNN training, and testing, were conducted in MATLAB R2023a on a system equipped with an Intel Core i7-13700H CPU, 16 GB RAM, and Windows 11 Pro (64-bit).

The accuracy of BR-BPNN predictions across multiple time levels t is summarized in Tables 2, 3, and 4. These tables demonstrate consistently low error metrics for all solution types, confirming the model's robustness and fidelity in capturing the nonlinear wave dynamics encoded in the system (1.2). The graphical representations display the (1.2) solutions, highlighting the exact and neural network-predicted profiles for $\phi(x,t)$ and $\psi(x,t)$. In Figure 2a, the exact solution (3.9) reveals a localized wave structure with a dark peak propagating along the spatial axis x over time t, maintaining a stable

TABLE 2 | Statistical metrics by BR-BPNN for different t values.

Statistical metrics	$\phi(x,t)$					$\psi(x,t)$				
	$t=0.5$	$t=1$	$t=1.5$	$t=3$	$t=5$	$t=0.5$	$t=1$	$t=1.5$	$t=3$	$t=5$
RMSE	0.000255	0.00041291	0.00040395	0.00051929	0.0020338	4.3222e-06	5.6546e-06	2.3354e-06	5.5189e-06	5.3442e-06
MAE	8.8509e-05	0.00020364	0.00018409	0.00014336	0.00050532	3.8346e-06	5.0335e-06	2.0604e-06	4.4639e-06	4.1427e-06
MAPE	0.00080067	0.0013558	0.0012872	0.0016939	0.014802	0.00010246	0.00013788	4.5392e-05	0.00017957	0.00030819
MSE	6.5027e-08	1.7049e-07	1.6317e-07	2.6966e-07	4.1364e-06	1.8681e-11	3.1975e-11	5.4542e-12	3.0458e-11	2.8561e-11
R^2	1	1	1	0.99999	0.99988	1	1	1	1	1
R-score	1	1	1	1	1	1	1	1	1	1
rSD	1	1	0.99999	1.0003	1.0001	1	1	1	1	1
NSE	1	1	0.99999	0.99999	0.99997	1	1	1	1	1

TABLE 3 | Statistical metrics by BR-BPNN for different t values.

Statistical metrics	$\phi(x,t)$					$\psi(x,t)$				
	$t=0.5$	$t=1$	$t=1.5$	$t=3$	$t=5$	$t=0.5$	$t=1$	$t=1.5$	$t=3$	$t=5$
RMSE	0.000255	0.00041291	0.00040395	0.00095567	0.00088324	8.933e-05	4.2544e-05	1.6987e-06	1.2285e-05	7.4318e-06
MAE	8.8509e-05	0.00020364	0.00018409	0.00045173	0.00046924	4.3076e-05	3.5817e-05	1.3794e-06	9.631e-06	3.2164e-06
MAPE	0.00080067	0.0013558	0.0012872	0.010518	0.017158	0.025131	0.026341	0.00079057	0.0089716	0.002957
MSE	6.5027e-08	1.7049e-07	1.6317e-07	9.1331e-07	7.8011e-07	7.9798e-09	1.81e-09	2.8856e-12	1.5092e-10	5.5232e-11
R^2	1	1	1	0.99999	0.99999	1	1	1	1	1
R-score	1	1	1	1	1	1	1	1	1	1
rSD	1	1	0.99999	1.0002	0.99992	1	1	1	1	1
NSE	0.99999	0.99999	1	1	0.99999	1	1	1	1	1

TABLE 4 | Statistical metrics by BR-BPNN for different t values.

Statistical metrics	$\phi(x,t)$					$\psi(x,t)$				
	$t=0.5$	$t=1$	$t=1.5$	$t=3$	$t=5$	$t=0.5$	$t=1$	$t=1.5$	$t=3$	$t=5$
RMSE	1.4818e-06	3.4272e-06	4.5132e-06	1.148e-06	1.6704e-05	8.4127e-05	5.2629e-05	6.9054e-05	2.4512e-05	5.6902e-05
MAE	1.2859e-06	2.9841e-06	3.693e-06	1.0009e-06	1.4426e-05	4.6054e-05	1.6836e-05	2.6672e-05	6.8514e-06	2.2913e-05
MAPE	4.2202e-06	9.6805e-06	9.9394e-06	3.701e-06	6.0038e-05	0.007283	0.013071	0.011849	0.0075723	0.0062464
MSE	2.1959e-12	1.1745e-11	2.0369e-11	1.3179e-12	2.7901e-10	7.0774e-09	2.7698e-09	4.7685e-09	6.0083e-10	3.2378e-09
R^2	1	1	1	1	1	1	1	1	1	1
R-score	1	1	1	1	1	1	1	1	1	1
rSD	1	1	1	1	1	1	1	1	1	1
NSE	1	1	1	1	1	1	1	1	1	1

amplitude and shape. This behavior reflects the non-dispersive nature of the solution, as indicated by its hyperbolic and exponential terms. Similarly, Figure 2b presents the BR-BPNN-predicted solution for (3.9), closely matching the exact solution, capturing its spatio-temporal features with high precision. In Figure 3a, the exact solution (3.10) exhibits a comparable wave structure, with amplitude and phase variations determined by its analytical form. The corresponding BR-BPNN-predicted solution in Figure 3b aligns closely with the exact profile, demonstrating the neural network's effectiveness in approximating complex wave dynamics. These solutions represent traveling waves with soliton-like characteristics, preserving their shape and amplitude over time. This is particularly significant in practical applications such as optical fibers, plasma physics, and shallow-water wave phenomena. The strong agreement between the exact and predicted solutions further illustrates the utility of machine learning approaches like BR-BPNN in solving and analyzing nonlinear equations, especially in cases where traditional analytical methods are computationally expensive. The figures also capture intricate oscillatory and modulated structures of the wave solutions to the Shynaray-IIA equation. In Figure 4a, the solution (3.11) exhibits periodic waveforms that propagate coherently in both space and time, characterized by sharp, evenly spaced peaks and troughs, indicating undistorted propagation. Figure 5a displays the behavior of (3.12),

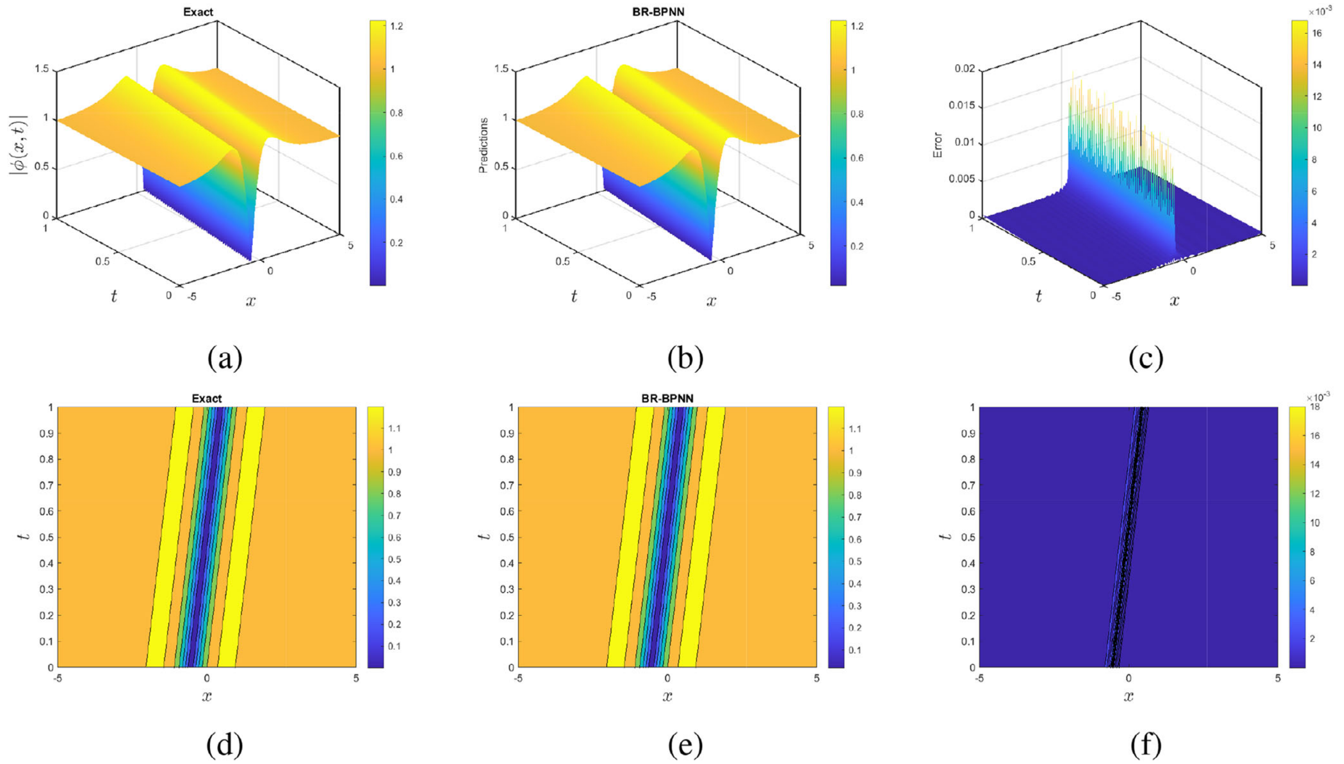

FIGURE 2 | Figures of (3.9) are provided for the constants as follows, $S_1 = 1$, $S_2 = 2$, $\tau = -1$, $\nu = 1$, $\varphi = -1$, $\gamma = 1$, $\beta = 1$, and $\omega_1 = 1$. [Colour figure can be viewed at wileyonlinelibrary.com]

where the amplitude varies periodically, forming an envelope around the oscillations. This modulation highlights the nonlinear effects, with the peaks and valleys of the envelope indicating regions of constructive and destructive interference. These features demonstrate the interplay between oscillatory dynamics and spatial modulation, which is central to the nonlinear nature of (1.2). When comparing the exact solutions with the BR-BPNN-predicted solutions, it is evident that the neural network successfully reproduces the primary structural features of both (3.11) and (3.12), including periodicity, amplitude, and modulation patterns. Minor deviations, especially in regions with rapid variations, suggest a smoothing effect in the predicted solutions, a known characteristic of neural network approximations. Finally, Figures 6a and 7a depict the solutions for (3.13) and (3.14), respectively, where (3.13) is shown to exhibit a bright soliton. The exact solution (3.13) in Figure 7a and its BR-BPNN-predicted counterpart in Figure 7b reveal a stable, non-dispersive wave profile that is a hallmark of soliton solutions to the (1.2). This wave maintains its form as it propagates, balancing the nonlinearities of the medium with the dispersive effects. The exact and predicted solutions (3.13) align closely, confirming the neural network's ability to accurately capture the soliton's dynamics. Bright solitons are important in practical applications because they can carry data without distortion or energy loss, which makes them ideal for information-transmission applications like optical fibers and communication systems. For high-speed, long-distance communications, the bright soliton's stability guarantees that transmitted signals stay steady over extended distances. Bright solitons are also crucial for plasma physics, which controls the dynamics of wave propagation in ionized gases, and nonlinear optics, which stabilizes pulses in fiber lasers. For cutting-edge technical applications that require precise control over wave behavior, the ability of solitons to maintain their shape while transmitting energy is particularly valuable. This discussion focuses on the solutions obtained using the $\left(\frac{G'}{G}, \frac{1}{G}\right)$–expansion method, where these solutions share a diverse form such as sech, tanh, and others. While this method is effective for generating a wide range of solutions, it does not provide a hierarchy of solutions that can be computed with other techniques like the Hirota bilinear method or the Darboux dressing method. Nonetheless, it remains highly useful for generating various types of solutions, including bright, dark, kink, and rational solutions, using the $\left(\frac{G'}{G}, \frac{1}{G}\right)$– expansion method.

To further support the robustness of the derived soliton solutions, we briefly examine their spectral stability. Let us consider perturbed solutions of the form:

$$\phi(x,t) = \phi_0(x,t) + \delta\ \phi_1(x,t), \quad \psi(x,t) = \psi_0(x,t) + \delta\ \psi_1(x,t),$$

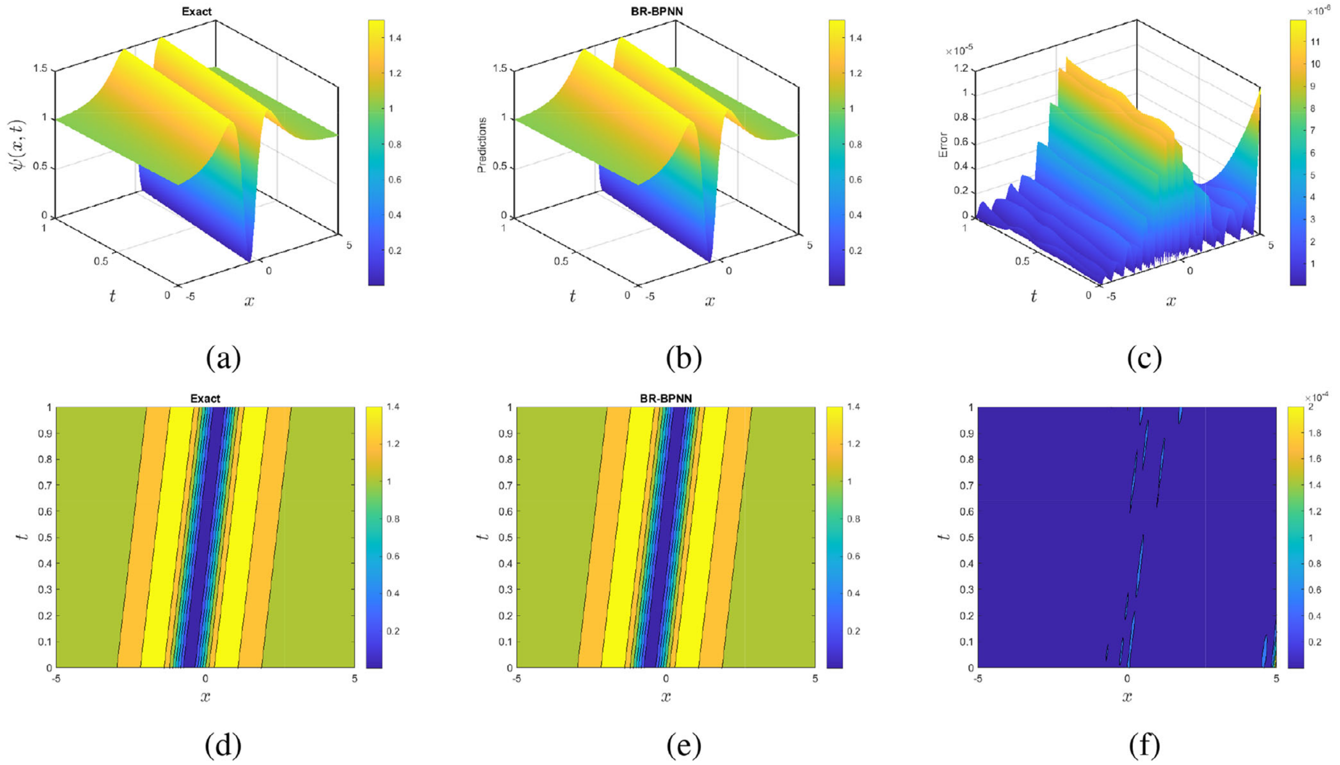

FIGURE 3 | Figures of (3.10) are provided for the constants as follows, $S_1 = 1,\ S_2 = 2,\ \tau = -1,\ \nu = 1,\ \varphi = -1,\ \gamma = 1,\ \beta = 1$, and $\omega_1 = 1$. [Colour figure can be viewed at wileyonlinelibrary.com]

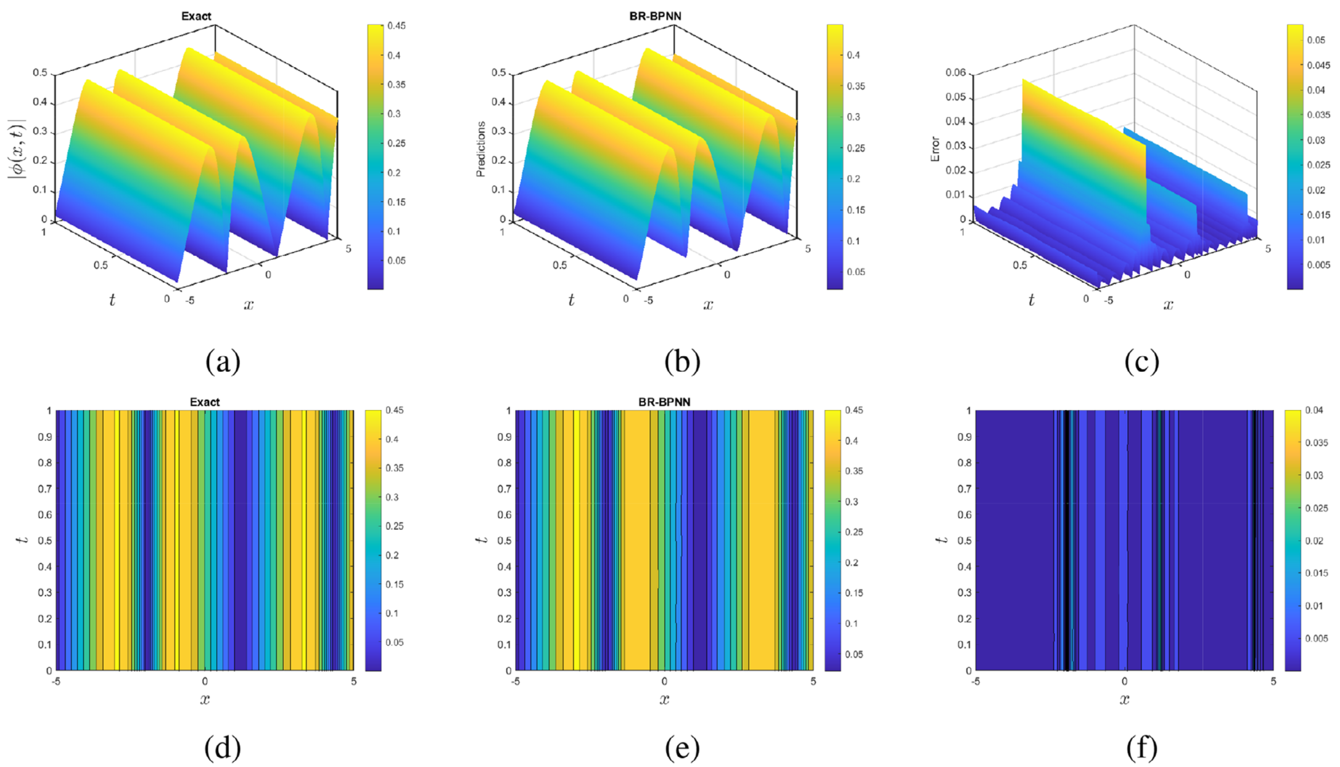

FIGURE 4 | Figures of (3.11) are provided for the constants as follows, $S_1 = 1,\ S_2 = 2,\ \tau = -1,\ \nu = 1,\ \varphi = -1,\ \gamma = 1,\ \beta = 1$, and $\omega_1 = 1$. [Colour figure can be viewed at wileyonlinelibrary.com]

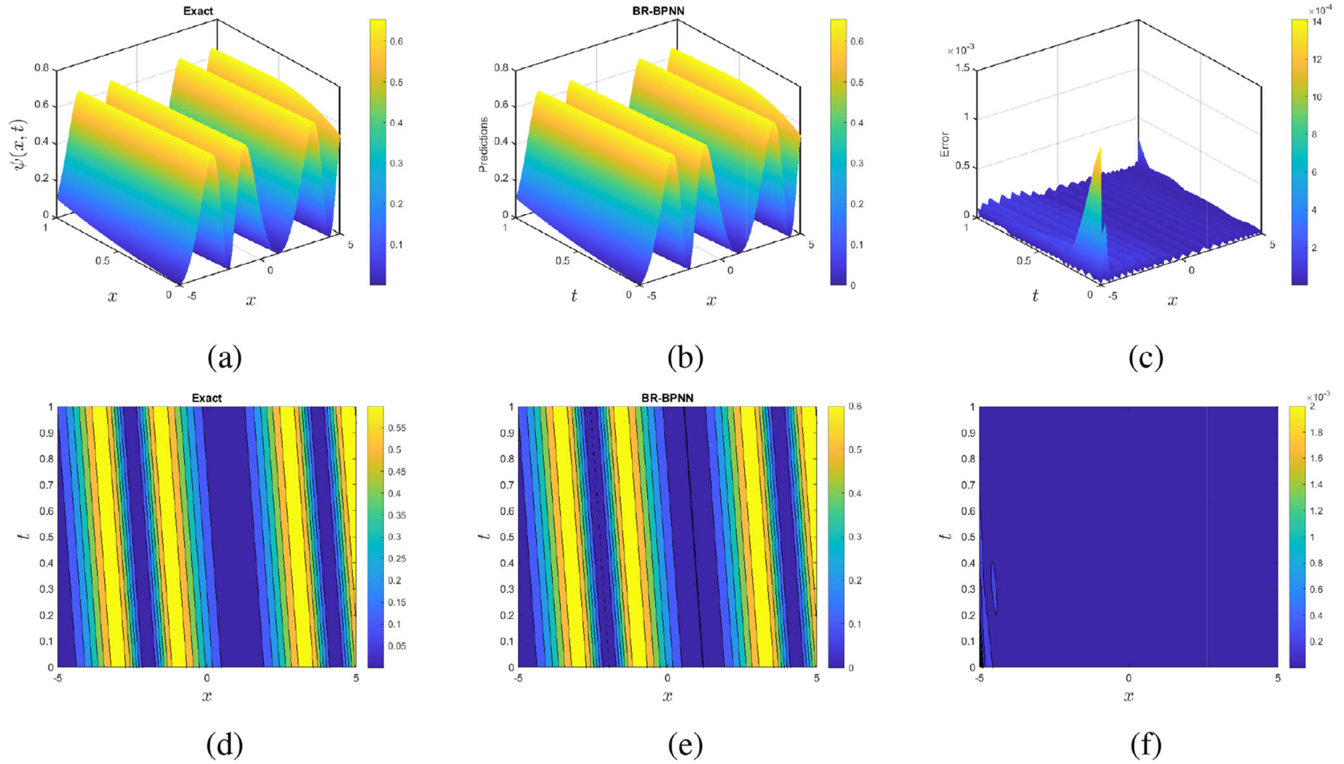

FIGURE 5 | Figures of (3.12) are provided for the constants as follows, $S_1 = 1,\ S_2 = 2,\ \tau = -1,\ \nu = 1,\ \varphi = -1,\ \gamma = 1,\ \beta = 1$, and $\omega_1 = 1$. [Colour figure can be viewed at wileyonlinelibrary.com]

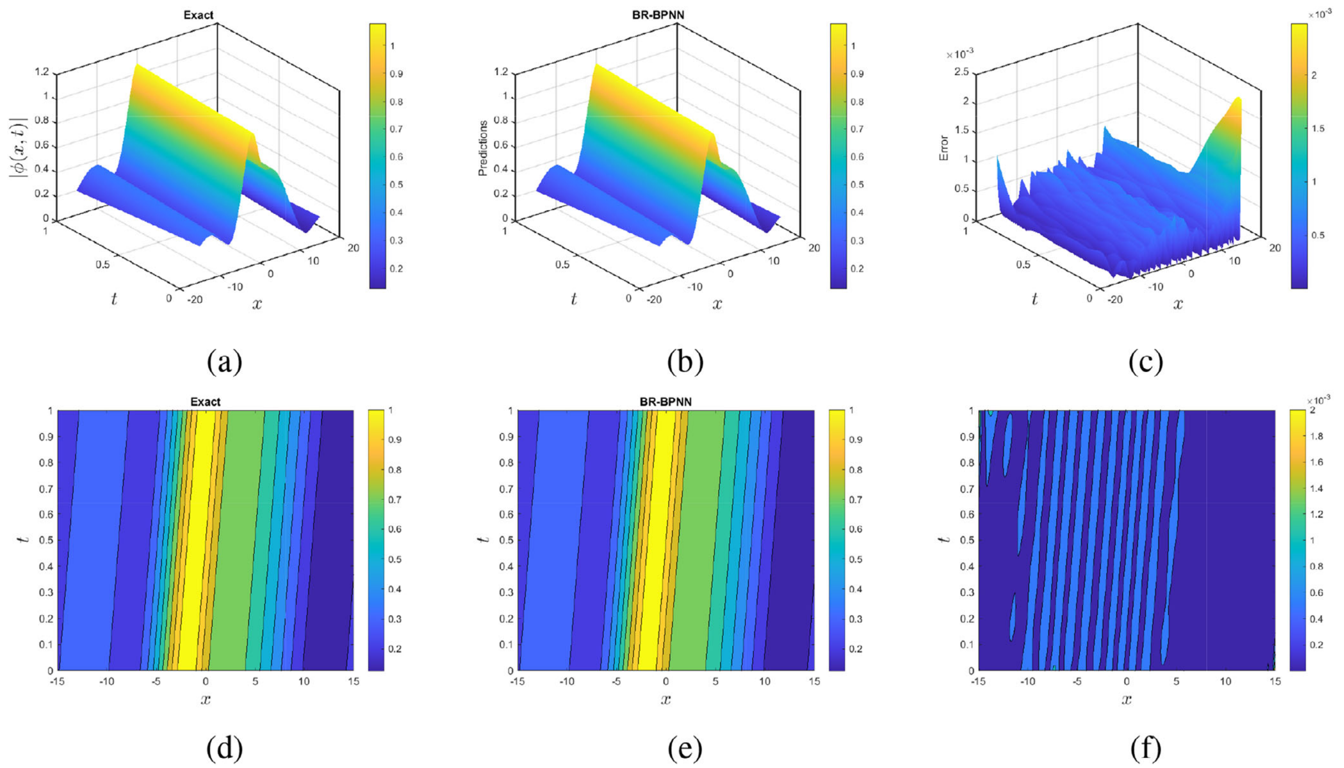

FIGURE 6 | Figures of (3.13) are provided for the constants as follows, $S_1 = 1,\ S_2 = 2,\ \tau = -1,\ \nu = 1,\ \varphi = -1,\ \gamma = 1,\ \beta = 1$, and $\omega_1 = 1$. [Colour figure can be viewed at wileyonlinelibrary.com]

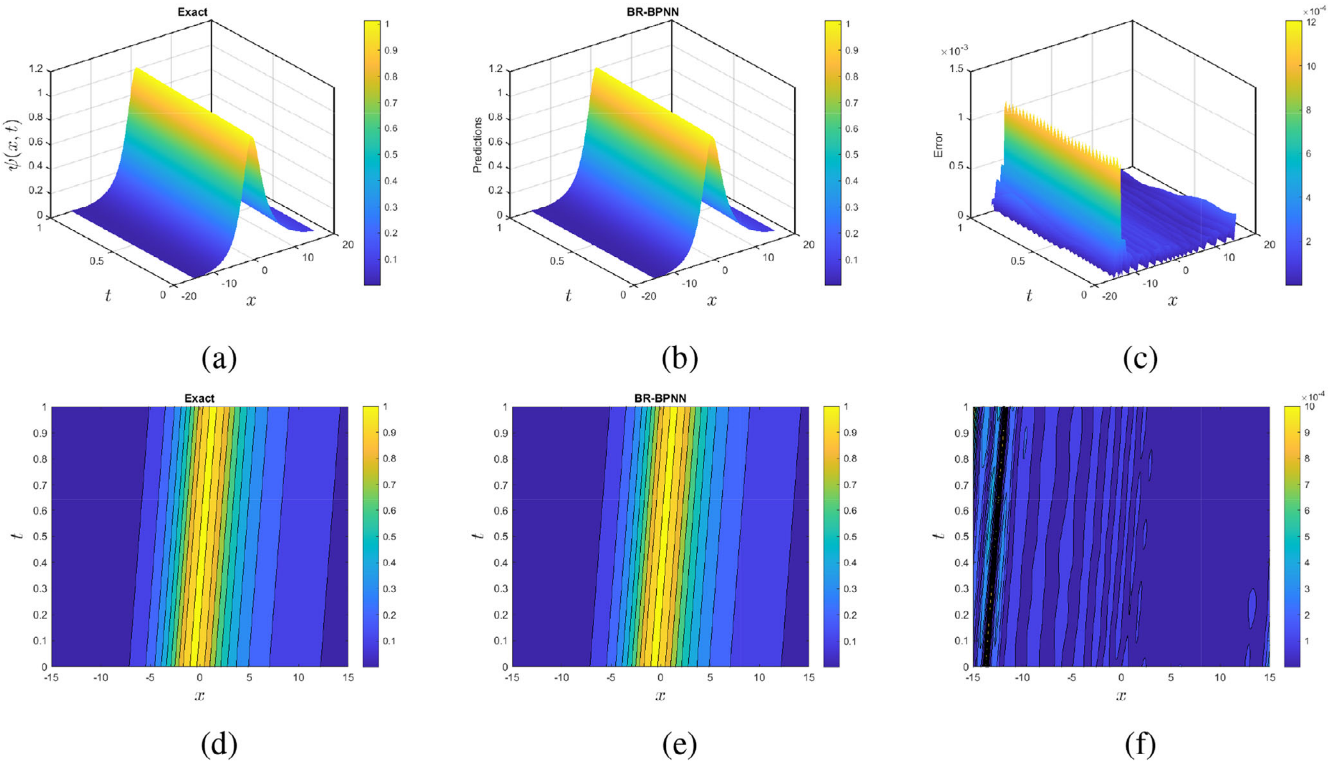

FIGURE 7 | Figures of (3.14) are provided for the constants as follows, $S_1 = 1,\ S_2 = 2,\ \tau = -1,\ \nu = 1,\ \varphi = -1,\ \gamma = 1,\ \beta = 1$, and $\omega_1 = 1$. [Colour figure can be viewed at wileyonlinelibrary.com]

where ϕ_0 and ψ_0 are seed solutions, and $\delta \ll 1$ denotes a small perturbation. Substituting into the (1.2) and linearizing in δ leads to a coupled system of linear PDEs for the perturbation fields ϕ_1 and ψ_1. The spectral stability is determined by examining the eigenvalues of the associated linearized operator: spectral stability holds if all eigenvalues have non-positive real parts. While a rigorous spectral decomposition is beyond the scope of this work, the numerical results shown in Tables 2–4 and their associated figures provide strong evidence of stability. The soliton profiles maintain their structure and amplitude over time, both in analytical and BR-BPNN-predicted cases. The absence of any visible growth in the error profiles suggests that the soliton families investigated, particularly the bright solitons, are spectrally stable under small disturbances.

5 | Conclusion

This study applied the $\left(\frac{G'}{G}, \frac{1}{G}\right)$-expansion method to successfully generate new soliton solutions of the Shynaray-IIA equation, showing that this method is useful for obtaining exact solutions of nonlinear partial differential equations. The results from the BR-BPNN model matched closely with the exact solutions, confirming the accuracy and efficiency of the proposed numerical approach. Several statistical error metrics were used to evaluate the performance of the model, and a strong correlation between analytical and predicted solutions was observed. This supports the idea that combining traditional analytical techniques with machine learning tools can be effective for solving complex nonlinear problems. The main contribution of this work is the development of a combined analytical and neural network-based framework for solving the Shynaray-IIA equation, which has not been addressed in previous studies. This work provides a simple and effective approach for analyzing nonlinear systems and can be extended to other equations in applied science and engineering.

While the findings of this study are insightful, there are several promising avenues for future exploration. To further validate the reliability of the $\left(\frac{G'}{G}, \frac{1}{G}\right)$-expansion method, one approach could be to extend it to more complex systems, such as higher-dimensional equations or those with variable coefficients. Additionally, the BR-BPNN model could be improved by investigating different architectures, including deeper or more specialized networks, to enhance prediction accuracy for more intricate systems. Furthermore, examining alternative machine learning techniques, such as physics-informed neural networks, may increase both training efficiency and predictive power. Finally, future research could focus on developing hybrid models that combine analytical and numerical methods with advanced machine learning to solve highly non-linear, time-dependent equations, paving the way for more advanced and accurate modeling in various fields.

Author Contributions

Aamir Farooq: conceptualization, data curation, formal analysis, writing – original draft. **H. W. A. Riaz:** conceptualization, formal Analysis, writing – review and editing. **Sadique Rehman:** formal analysis, writing – review and editing. **M. Mamun Miah:** data curation, formal analysis, review and editing. **Wen Xiu Ma:** writing – review and editing.

Acknowledgments

Aamir Farooq acknowledges the postdoctoral fellowship supported by Zhejiang Normal University, China, under Grant No. YS304024913. Wen-Xiu Ma acknowledges support from the Ministry of Science and Technology of China (G2021016032L and G2023016011L), the National Natural Science Foundation of China (NSFC) under grants 12271488 and 11975145, and the Natural Science Foundation for Colleges and Universities in Jiangsu Province (17KJB110020).

Funding

This work was supported by the Natural Science Foundation for Colleges and Universities in Jiangsu Province, the Ministry of Science and Technology of the People's Republic of China, the National Natural Science Foundation of China, and a postdoctoral fellowship supported by Zhejiang Normal University.

Conflicts of Interest

The authors declare no conflicts of interest.

Data Availability Statement

All data are available within the article.

References

1. Z. Sagidullayeva, G. Nugmanova, R. Myrzakulov, and N. Serikbayev, "Integrable Kuralay Equations: Geometry, Solutions and Generalizations," *Symmetry* 14, no. 7 (2022): 1374.

2. Z. Sagidullayeva, K. Yesmakhanova, G. Nugmanova, and R. Myrzakulov, "Soliton Solutions of the Kuralay Equation via Hirota Bilinear Method," in *Proceedings of the 6th NMMP-2022, FAMU, Tallahassee, FL, USA*, 2022, pp. 17–19.

3. L. Debnath and L. Debnath, *Nonlinear Partial Differential Equations for Scientists and Engineers* (Springer, 2005).

4. S. Zhang and L. Yi, "Exact Solutions of a Generalized Nonlinear schrödinger Equation," *Physical Review E: Statistical, Nonlinear, and Soft Matter Physics* 78, no. 2 (2008): 026602.

5. Z. Dai, J. Liu, and Z. Liu, "Exact Periodic Kink-Wave and Degenerative Soliton Solutions for Potential Kadomtsev–Petviashvili Equation," *Communications in Nonlinear Science and Numerical Simulation* 15, no. 9 (2010): 2331–2336.

6. M. Wang, X. Li, and J. Zhang, "The (g'/g)-Expansion Method and Travelling Wave Solutions of Nonlinear Evolution Equations in Mathematical Physics," *Physics Letters A* 372, no. 4 (2008): 417–423.

7. Q. Zhou, M. E. H. M. E. T. Ekici, A. B. D. U. L. L. A. H. Sonmezoglu, and M. Mirzazadeh, "Optical Solitons With Biswas–Milovic Equation by Extended $(g'/g$-Expansion Method," *Optik* 127, no. 16 (2016): 6277–6290.

8. Y. Yildirim, A. Biswas, M. Ekici, et al., "Optical Solitons in Birefringent Fibers for Radhakrishnan–Kundu–Lakshmanan Equation With Five Prolific Integration Norms," *Optik* 208 (2020): 164550.

9. M. I. Khan, J. Sabi'u, A. Khan, S. Rehman, and A. Farooq, "Unveiling New Insights Into Soliton Solutions and Sensitivity Analysis of the Shynaray-Iia Equation Through Improved Generalized Riccati Equation Mapping Method," *Optical and Quantum Electronics* 56, no. 8 (2024): 1339.

10. G. H. Tipu, W. A. Faridi, D. Rizk, Z. Myrzakulova, R. Myrzakulov, and L. Akinyemi, "The Optical Exact Soliton Solutions of Shynaray-Iia Equation With ϕ 6-Model Expansion Approach," *Optical and Quantum Electronics* 56, no. 2 (2024): 226.

11. Y. S. Özkan, "The Exact Solutions of the Shynaray-Iia Equation Along With Analysis of Bifurcation and Chaotic Behaviors," *Qualitative Theory of Dynamical Systems* 23, no. Suppl 1 (2024): 288.

12. D. Chou, H. U. Rehman, A. Amer, and M. S. Osman, "Optical Soliton Dynamics of the Conformable Nonlinear Evolution Equation in Bose–Einstein Condensates," *Rendiconti Lincei. Scienze Fisiche e Naturali* 35 (2024): 1–12.

13. A. Biswas, Y. Yildirim, E. Yaşar, Q. Zhou, S. P. Moshokoa, and M. Belic, “Optical Soliton Perturbation With Quadratic-Cubic Nonlinearity Using a Couple of Strategic Algorithms,” *Chinese Journal of Physics* 56, no. 5 (2018): 1990–1998.

14. A. Darwish, E. A. El-Dahab, H. Ahmed, et al., “Optical Solitons in Fiber Bragg Gratings via Modified Simple Equation,” *Optik* 203 (2020): 163886.

15. E. Fan, “Uniformly Constructing a Series of Explicit Exact Solutions to Nonlinear Equations in Mathematical Physics,” *Chaos, Solitons & Fractals* 16, no. 5 (2003): 819–839.

16. N. A. Kudryashov, A. Biswas, A. G. Borodina, Y. Yildirim, and H. M. Alshehri, “Painlevé Analysis and Optical Solitons for a Concatenated Model,” *Optik* 272 (2023): 170255.

17. D. Chou, H. U. Rehman, A. Amer, and A. Amer, “New Solitary Wave Solutions of Generalized Fractional tzitzéica-Type Evolution Equations Using Sardar Sub-Equation Method,” *Optical and Quantum Electronics* 55, no. 13 (2023): 1148.

18. H. U. Rehman, G. S. Said, A. Amer, et al., “Unraveling the (4+ 1)-dimensional Davey-Stewartson-Kadomtsev-Petviashvili Equation: Exploring Soliton Solutions via Multiple Techniques,” *Alexandria Engineering Journal* 90 (2024): 17–23.

19. A. Biswas, Y. Yildirim, E. Yasar, et al., “Optical Soliton Perturbation With Full Nonlinearity by Trial Equation Method,” *Optik* 157 (2018): 1366–1375.

20. Y. Yildirim, “Optical Solitons of Biswas-Arshed Equation in Birefringent Fibers by Trial Equation Technique,” *Optik* 182 (2019): 810–820.

21. M. Tahir, A. U. Awan, and H. u. Rehman, “Optical Solitons to Kundu–Eckhaus Equation in Birefringent Fibers Without Four-Wave Mixing,” *Optik* 199 (2019): 163297.

22. Y. Yildirim and E. Yaşar, “A (2+ 1)-dimensional Breaking Soliton Equation: Solutions and Conservation Laws,” *Chaos, Solitons & Fractals* 107 (2018): 146–155.

23. L.-x. Li, E.-q. Li, and M.-l. Wang, “The $\left(\frac{G'}{G}, \frac{1}{G}\right)$-Expansion Method and Its Application to Travelling Wave Solutions of the Zakharov Equations,” *Applied Mathematics-A Journal of Chinese Universities* 25 (2010): 454–462.

24. W. A. Faridi, G. H. Tipu, Z. Myrzakulova, R. Myrzakulov, and L. Akinyemi, “Formation of Optical Soliton Wave Profiles of Shynaray-Iia Equation via Two Improved Techniques: A Comparative Study,” *Optical and Quantum Electronics* 56, no. 1 (2024): 132.

25. M. I. Khan, D. N. K. Marwat, J. Sabi’u, and Mustafa Inc, “Exact Solutions of Shynaray-Iia Equation (s-Iiae) Using the Improved Modified Sardar Sub-Equation Method,” *Optical and Quantum Electronics* 56, no. 3 (2024): 459.

26. A. Altalbe, A. Taishiyeva, R. Myrzakulov, A. Bekir, and A. A. Zaagan, “Effect of Truncated m-Fractional Derivative on the New Exact Solitons to the Shynaray-Iia Equation and Stability Analysis,” *Results in Physics* 57 (2024): 107422.

27. W. S. McCulloch and W. Pitts, “A Logical Calculus of the Ideas Immanent in Nervous Activity,” *Bulletin of Mathematical Biophysics* 5 (1943): 115–133.

28. G. Cybenko, “Approximation by Superpositions of a Sigmoidal Function,” *Mathematics of Control, Signals, and Systems* 2, no. 4 (1989): 303–314.

29. K. Hornik, M. Stinchcombe, and H. White, “Multilayer Feedforward Networks Are Universal Approximators,” *Neural Networks* 2, no. 5 (1989): 359–366.

30. B. Adcock and N. Dexter, “The Gap Between Theory and Practice in Function Approximation With Deep Neural Networks,” *SIAM Journal on Mathematics of Data Science* 3, no. 2 (2021): 624–655.

31. X. Li, “Simultaneous Approximations of Multivariate Functions and Their Derivatives by Neural Networks With One Hidden Layer,” *Neurocomputing* 12, no. 4 (1996): 327–343.

32. M. Raissi, P. Perdikaris, and G. E. Karniadakis, “Physics-Informed Neural Networks: A Deep Learning Framework for Solving Forward and Inverse Problems Involving Nonlinear Partial Differential Equations,” *Journal of Computational Physics* 378 (2019): 686–707.

33. H. W. A. Riaz and A. Farooq, “Solitonic Solutions for the Reduced Maxwell-Bloch Equations via the Darboux Transformation and Artificial Neural Network in Nonlinear Wave Dynamics,” *Physica Scripta* 99 (2024): 126010.

34. H. W. A. Riaz and A. Farooq, “A (2+ 1) Modified Kdv Equation With Time-Dependent Coefficients: Exploring Soliton Solution via Darboux Transformation and Artificial Neural Network Approach,” *Nonlinear Dynamics* 113 (2024): 1–17.

35. A. Waheed, M. Awais, M. A. Z. Raja, M. Y. Malik, and A. S. Alqahtani, “Peakon and Solitary Wave Solutions of the Lax Equation: Neuro Computing Procedure,” *International Communications in Heat and Mass Transfer* 152 (2024): 107321.

36. J. Vyas, R. Kohli, S. Gupta, and H. Pothukuchi, “Liquid Droplet Entrainment in an Annular Flow Boiling Regime—A Bayesian Regularization Algorithm Based Study,” *Journal of Applied Physics* 135, no. 16 (2024).

37. S. V. S. S. N. V. G. Sumant Kumar, B. V. Krishna Murthy, R. Kumar, and D. Parmar, “Multi-Physics Study on Double-Diffusion Convective Flow in an Inverted t-Shaped Porous Enclosure: Ann-Based Parametric Estimation,” *Physics Letters A* 518 (2024): 129681.

38. M. N. Hossain, M. Mamun Miah, F. Z. Duraihem, and S. Rehman, "Stability, Modulation Instability, and Analytical Study of the Confirmable Time Fractional Westervelt Equation and the Wazwaz Kaur Boussinesq Equation," *Optical and Quantum Electronics* 56, no. 6 (2024): 1–29.

39. M. A. Iqbal, D. Baleanu, M. M. Miah, H. M. S. Ali, H. M. Alshehri, and M. S. Osman, "New Soliton Solutions of the Mzk Equation and the Gerdjikov-Ivanov Equation by Employing the Double $(G'/G, 1/G)$-Expansion Method," *Results in Physics* 47, no. 47 (2023): 106391.

40. M. A. Iqbal, M. Ye Wang, M. Miah, and M. S. Osman, "Study on Date–Jimbo–Kashiwara–Miwa Equation With Conformable Derivative Dependent on Time Parameter to Find the Exact Dynamic Wave Solutions," *Fractal and Fractional* 6, no. 1 (2021): 4.

41. M. T. Hagan, H. B. Demuth, and M. Beale, *Neural Network Design* (PWS Publishing Co., 1997).

42. D. J. C. MacKay, "A Practical Bayesian Framework for Backpropagation Networks," *Neural Computation* 4, no. 3 (1992): 448–472.

43. F. Burden and D. Winkler, "Bayesian Regularization of Neural Networks," in *Artificial Neural Networks: Methods and Applications* (Humana Press, 2009), 23–42.

44. F. Dan Foresee and M. T. Hagan, "Gauss-Newton Approximation to Bayesian Learning," in *Proceedings of International Conference on Neural Networks (ICNN'97)*, volume 3, 1997, pp. 1930–1935. IEEE.

Appendix A

Symbolic Verification

The following `Maple` code was used to symbolically verify that the function $T(\chi)$ satisfies the ordinary differential equation derived from the Shynaray-IIA system (1.2). The code confirms that the resulting expression simplifies to zero under the specified parameter relations.

$$\text{restart};\quad \text{with(student)}:$$

$$\text{assume}\left(0 < p,\ \tau < 0,\ 0 < \omega,\ 0 < \zeta,\ 0 < l,\ \upsilon \in \mathbb{R},\ \omega_1 \in \mathbb{R}\right):$$

$$\text{rel}_1 := \begin{cases} a = \dfrac{2\,(F\,\omega - F)}{\tau}, \\ d_0 = 0, \\ d_1 = \dfrac{\sqrt{p}}{l\,\sqrt{2\,\omega\,\zeta}}, \\ e_1 = \dfrac{\sqrt{p\left(\tau^2\omega_1 + \upsilon^2\right)}}{l\,\sqrt{-\tau}\,\sqrt{2\,\omega\,\zeta}} \end{cases}$$

$$T = \frac{\sqrt{-p\,\tau}\,\left(S_1\cosh(\sqrt{-\tau}\,\chi) + S_2\sinh(\sqrt{-\tau}\,\chi)\right)}{l\,\sqrt{2\,\omega\,\zeta}\,\left(S_1\sinh(\sqrt{-\tau}\,\chi) + S_2\cosh(\sqrt{-\tau}\,\chi) + \frac{\upsilon}{\tau}\right)} + \frac{\sqrt{p\left(\tau^2\omega_1 + \upsilon^2\right)}}{l\,\sqrt{-\tau}\,\sqrt{2\,\omega\,\zeta}\,\left(S_1\sinh(\sqrt{-\tau}\,\chi) + S_2\cosh(\sqrt{-\tau}\,\chi) + \frac{\upsilon}{\tau}\right)}$$

$$\text{expr} := a\,\frac{\partial^2 T}{\partial\chi^2} + F(1-\omega)T - \frac{\omega\,\zeta\,a\,l^2\,T^3}{p}$$

$$\text{expr}_{\text{sub}} := \text{eval}\left(\text{expr}, \text{rel}_1\right)$$

$$\text{expr}_{\text{final}} := \text{simplify}\left(\text{subs}\{\omega_1 = S_1^2 - S_2^2\},\ \text{expr}_{\text{sub}}\right)$$

$$\text{is}\left(\text{expr}_{\text{final}} = 0\right) \quad \Rightarrow \quad \text{true}$$

This computation confirms that the expression for $T(\chi)$ in (3.8) is indeed an exact solution of the reduced equation, validating the analytical results presented in Section 3.1. Similarly, other solutions can be verified in the same manner.